Journal of Power Sources 214 (2012) 298–302

Contents lists available at SciVerse ScienceDirect

Journal of Power Sources

journal homepage: www.elsevier.com/locate/jpowsour

Short communication

Mesoporous titania rods as an anode material for high performance lithium-ion batteries

Yan-Mei Jiang, Kai-Xue Wang*, Xing-Xing Guo, Xiao Wei, Jing-Feng Wang, Jie-Sheng Chen*

School of Chemistry and Chemical Engineering, Shanghai Jiao Tong University, 800 Dongchuan Road, Shanghai 200240, China

HIGHLIGHTS

- Mesoporous anatase TiO_2 rods have been synthesized by ultraviolet irradiation and subsequent calcination processes.
- The unique mesoporous structure and the crystal nature of the rods ensure fast Li^+ insertion/extraction kinetics.
- Mesoporous TiO_2 rods with high electrochemical performance are promising anode materials for lithium-ion batteries.

ARTICLE INFO

Article history:
Received 3 April 2012
Received in revised form
25 April 2012
Accepted 27 April 2012
Available online 4 May 2012

Keywords:
Light-driven process
Anatase titania
Mesoporous structure
Lithium-ion batteries

ABSTRACT

Mesoporous TiO_2 rods consisting of anatase nanoparticles have been successfully prepared via the calcination of a porous amorphous TiO_2 precursor obtained by ultraviolet irradiation of titanium glycolate. The product is characterized by X-ray diffraction, nitrogen adsorption-desorption, electron microscopy. The electrochemical properties of the material are evaluated by cyclic voltammetry (CV) and galvanostatic charge and discharge measurements. It is found that the initial lithium insertion/extraction capacities of the material reach 262 and 221 mAh g^{-1}, respectively, at a current density of 0.1 A g^{-1}. A discharge capacity of approximately 161 mAh g^{-1} can be retained after the material is cycled at 1.0 A g^{-1} for 40 cycles, demonstrating good rate performance and high cycleability. The high electrochemical performance of the anatase rods is ascribed to the unique mesoporous structure and the crystalline nature of the rods. This mesoporous TiO_2 with a rod shape is promising for use as an anode material for lithium-ion batteries with high power and energy densities.

1. Introduction

New energy technologies promote the rapid development of low-carbon economy, and simultaneously put forward ever-increasing requirement for high performance batteries such as lithium-ion batteries (LIBs) [1]. One of the keys to the high performance of LIBs lies in the behavior of electrode materials. Since the first report by Ohzuku et al. in 1979 [2], TiO_2 anode material has received extensive attention [3–6]. The insertion reaction of Li^+ into TiO_2 electrode can be expressed as the following equation [7,8].

$$TiO_2 + xLi^+ \rightarrow xe^- \rightarrow Li_xTiO_2 \quad (1)$$

The maximum theoretical capacity of TiO_2 is 335 mAh g^{-1}, corresponding to $x = 1$ and the complete reduction of Ti^{4+} to Ti^{3+}. When used as anode material for LIBs, the anatase TiO_2 has many advantages over other materials such as the commercial carbons. First, the two-way channels parallel to *a* and *b* axes in the anatase TiO_2 [9] provide fast Li insertion/extraction pathways. Second, the negligible volume change of TiO_2 electrodes during the insertion/extraction of lithium ions guarantees good cycling stability of the batteries [10]. Thirdly, the high insertion voltage of the anatase TiO_2 can effectively avoid the formation of solid electrolyte interface (SEI) and lithium dendrites, ensuring good thermal stability and safety of the batteries [10]. Thus, anatase TiO_2 has been widely investigated as a key material for fundamental research and technological applications in the fields of LIBs [11–14]. However, the rate performance of TiO_2 is rather low because of the low electronic conductivity (EC), limiting their application in LIBs with high power densities [10]. Therefore, it is highly desirable to improve the rate performance of TiO_2. Mesoporous materials constructed by nanoparticles with an appropriate size may shorten the diffusion distance of lithium-ions. The two-dimensional or three-dimensional porous systems may facilitate the transportation of electrolyte and lithium-ions inside these materials [15–18]. For electrode materials with mesoporous structures, high rate capabilities are expected. Moreover, the

* Corresponding authors. Tel.: +86 21 3420 1273; fax: +86 21 5474 1297.
E-mail addresses: k.wang@sjtu.edu.cn (K.-X. Wang), chemcj@sjtu.edu.cn (J.-S. Chen).

0378-7753/$ – see front matter © 2012 Elsevier B.V. All rights reserved.
doi:10.1016/j.jpowsour.2012.04.091

capacity decay caused by the dissociation of nanoparticles from the electrode surface may be avoided as well. Thus, it might be a feasible way to improve the performance of TiO_2 by introducing a mesoporous structure to the material.

Herein, we describe the preparation of mesoporous TiO_2 rods composed of anatase nanoparticles through a rapid template-free approach based on ultraviolet light irradiation and subsequent calcination. These mesoporous anatase TiO_2 rods exhibit excellent electrochemical properties. The introduction of mesoporous structures through the light-driven formation pathway are proved to be efficient in improving the electrochemical properties of electrode materials for LIBs.

2. Experimental

The mesoporous anatase TiO_2 rods were obtained through the calcination of amorphous TiO_2 rods prepared following the procedure reported previously [19]. First, titanium glycolate was synthesized through the reaction of tetrabutyl titanate and ethylene glycol (1:100 by volume) at 160 °C for 2 h under vigorous stirring. Then, amorphous TiO_2 rods with porous structures were prepared via the irradiation of titanium glycolate in ultraviolet light under atmospheric pressure. Finally, the mesoporous anatase TiO_2 rods were obtained by the calcination of the amorphous TiO_2 rods in air at 500 °C for 5 h.

Powder X-ray diffraction (XRD) patterns were recorded on a Rigaku Dmax-2200 diffractometer (Rigaku, Japan) with Cu Kα radiation ($\lambda = 1.5418$ Å). The morphology of the sample was observed with a scanning electron microscope (SEM, JSM-7401F, JEOL, Japan). The microstructure of the sample was characterized by using transmission electron microscope (TEM, JEM-2100F, JEOL, Japan) and high resolution transmission electron microscope (HRTEM, JEM-2100F, JEOL, Japan), operating at 200 kV. The specific surface areas of the samples were measured on a Micromeritics ASAP 2010M + C nitrogen adsorption instrument (Micrometritices Inc., USA) at 77 K.

Electrochemical properties of the mesoporous anatase TiO_2 rods were evaluated with CR2016 coin cells. The working electrode was prepared on an aluminum foil by using a doctor-blade method with a slurry composed of 75 wt.% active materials (TiO_2), 15 wt.% conductivity agent (acetylene black), and 10 wt.% binder (polyvinylidene fluoride, PVDF). Lithium metal foil was used as both the counter and reference electrodes. A microporous polypropylene membrane (Celgard 2500) was used as the separator. Coin cells were assembled in an argon filled glove box with both moisture and oxygen contents below 1.0 ppm. The electrolyte was 1.0 M of $LiClO_4$ in ethylene carbonate/dimethyl carbonate (EC/DEC, 1:1 by volume). The galvanostatic charge and discharge experiment was performed with a battery tester LAND-CT2001A in the voltage range of 1.0–3.0 V at room temperature. The cyclic voltammograms (CV) were obtained on a CHI660B electrochemical workstation at a scanning rate of 0.2 mV s^{-1} in a potential range of 1.0 – 3.0 V (vs Li/Li^+).

3. Results and discussion

The X-ray diffraction (XRD) pattern of the TiO_2 rods is shown in Fig. 1a. The peaks located at approximately 25.4°, 37.9°, 48.1°, 54.0° and 55.1° can be readily indexed as the (101) (004) (200) (105), and (211) diffractions of tetragonal anatase phase of TiO_2 (JCPDS No. 21–1272). The XRD data indicate that pure tetragonal anatase with highly oriented (101) crystal plane is generated after the ultraviolet irradiation and the subsequent calcination. The average crystallite size is approximately 18 nm based on the calculation with Debye-Scherrer's equation.

The textural properties of the anatase rods has been characterized by nitrogen adsorption/desorption experiments performed at

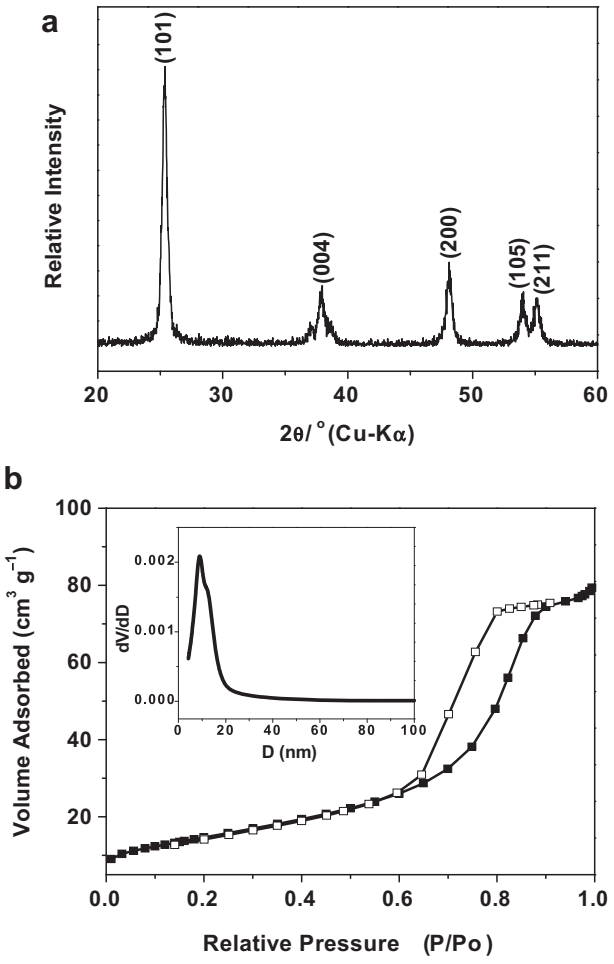

Fig. 1. XRD pattern (a) and N_2 adsorption–desorption isotherms (b) of mesoporous anatase TiO_2 rods (Inset: the pore size distribution curve).

77 K. Nitrogen adsorption/desorption isotherms and the corresponding Barrett-Joyner-Halenda (BJH) pore size distribution curves of the anatase TiO_2 are displayed in Fig. 1b. The isotherms are identified as of type IV, characteristic of materials with mesoporous structures. The specific Brunauer-Emmett-Teller (BET) surface area and the pore volume are determined to be 53 m^2 g^{-1} and 0.12 cm^3 g^{-1}, respectively. The narrow Gaussian pore size distribution curve indicates that the sample has relatively regular pore channels in the mesoporous region. The average pore size is approximately 9 nm.

The rod-like morphology of the anatase TiO_2 is revealed by the SEM and TEM observation (Fig. 2A and B). The diameters of these rods are in the range of 0.5–1.0 μm. The length of the rods is less than 10 μm. As reported previously, titanium glycolate prepared through the reaction of tetrabutyl titanate and ethylene glycol usually has a rod-like morphology [20]. The SEM and low-magnification TEM images indicate that the rod-like morphology is well preserved during the ultraviolet irradiation and the following calcination. Further information on the microstructure of these rods is provided by HRTEM investigations (Fig. 2c). It is seen that the rods are composed of highly crystalline TiO_2 nanoparticles. The particle size is within the range of 10–20 nm, and the interparticle voids among these TiO_2 nanoparticles result in a mesoporous structure with pore diameters of approximately 9 nm. The selected area electron diffraction (SAED) exhibits a ring-like pattern, indicating the polycrystalline nature of the TiO_2 rods. All the rings

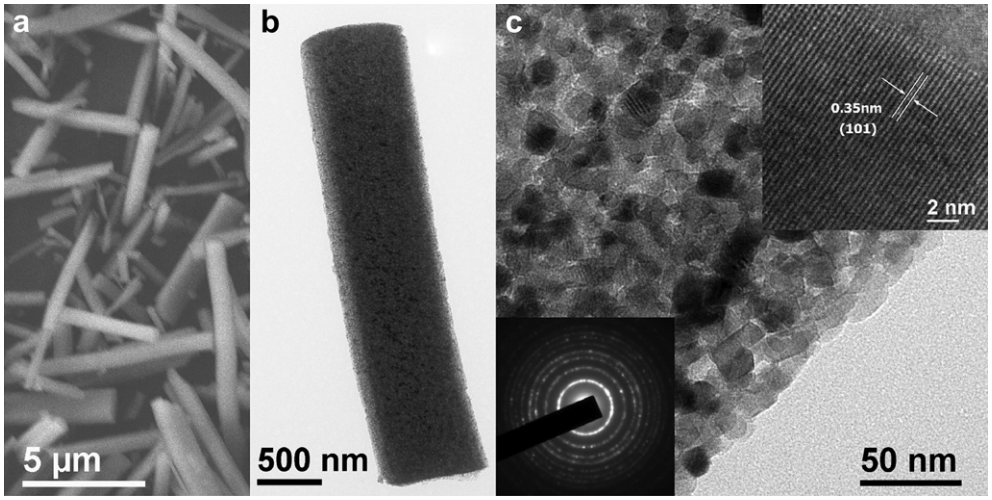

Fig. 2. SEM (a) and TEM images (b,c) of mesoporous anatase TiO_2 rods. The top right and bottom left insets in (c) are the HRTEM image and the corresponding SAED pattern of the anatase TiO_2, respectively.

can be well indexed as anatase phase, in consistence with the XRD results. Clear lattice fringes are observed in the HRTEM images (Inset in Fig. 2c). The interplanar spacing of approximately 0.35 nm is assigned to the (101) plane of anatase.

Anatase crystallizes in a tetragonal space group $I4_1/amd$ (No. 141). The Ti and O atoms occupy the 4a octahedral sites and 8e sites, respectively, resulting in interconnected lithium transport channels along the *a* and *b* axes. The crystal structure of anatase shown in Fig. 3 exhibits the lithium transport channels parallel to the *a* axis. During the discharge process, lithium ions move within the channels along *a* and *b* axes and occupy the empty 4b octahedral sites, leading to the formation of Li_xTiO_2 (Fig. 3). To elucidate the insertion/extraction of lithium-ions within the structure of anatase, cyclic voltammograms (CV) of the mesoporous TiO_2 rods were measured at a scan rate of 0.2 mV s^{-1} in the potential range from 3.0 to 1.0 V at room temperature (Fig. 4). The well-defined cathodic/anodic peaks located at 1.64 and 2.13 V (versus Li^+/Li) are associated with lithium-ion insertion/extraction within the anatase lattice, respectively. The potential interval of approximately 0.49 V between the cathodic and anodic peaks is consistent with that reported in the literature [21]. From the second cycle, the ratio of anodic to cathodic peak currents which is nearly 1 and the almost identical integral voltammetric area of the discharging/charging branches indicate that the insertion/extraction of lithium-ion in the mesoporous TiO_2 rods is highly reversible [22].

Fig. 5a displays the initial two discharge/charge curves of the mesoporous TiO_2 rods as the negative electrode with cutoff voltages of 3.0–1.0 V (versus Li^+/Li) at 0.1 A g^{-1} (approximately 0.6 C, 1 C = 168 mA g^{-1}). There are distinct potential plateaus at approximately 1.78 and 1.90 V for discharging and charging processes, corresponding to lithium-ion insertion/extraction within the anatase lattice, respectively. These plateaus are consistent with the cathodic and anodic peaks observed in the CV curve. In the discharge process, the potential drops dramatically first and then reaches a plateau at approximately 1.78 V, and finally gradually decreases to 1.0 V with a long sloped region. The initial potential drop above 1.78 V is attributed to a solid-solution insertion process [23]. The well-developed plateau at approximately 1.78 V is associated with the phase transition from tetragonal anatase TiO_2 to orthorhombic $Li_{0.5}TiO_2$. The following long slope between 1.78 and 1.0 V is ascribed to further lithium-ion insertion into $Li_{0.5}TiO_2$. The corresponding capacities of these regions in the initial two discharge/charge profiles are listed in Table 1. The total discharge capacity of the first cycle is approximately 262 mAh g^{-1}, corresponding to an insertion coefficient (x) of 0.78. The initial charge capacity is approximately 221 mAh g^{-1}, indicating a coulombic efficiency of 85% of the first cycle. The discharge/charge capacities of the second cycle are approximately 232

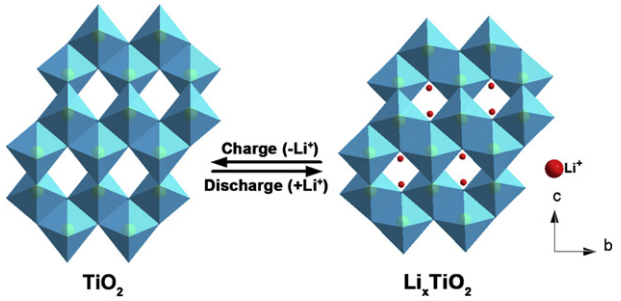

Fig. 3. Schematic representation illustrates the structural features of anatase TiO_2 upon Li^+ insertion/extraction.

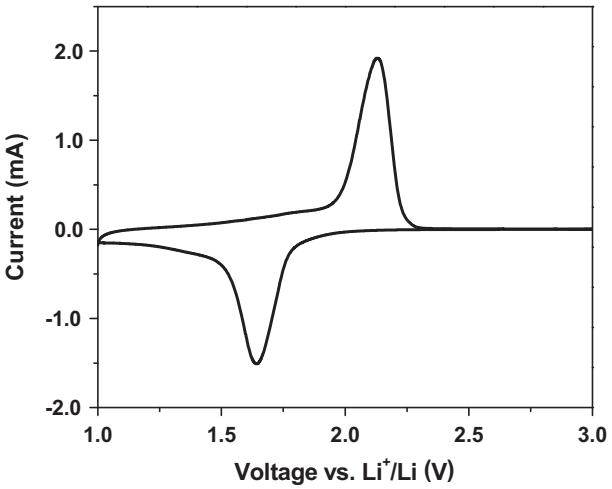

Fig. 4. Cyclic voltammogram of mesoporous anatase TiO_2 rods between 3.0 and 1.0 V with a scan rate of 0.2 mV s^{-1}.

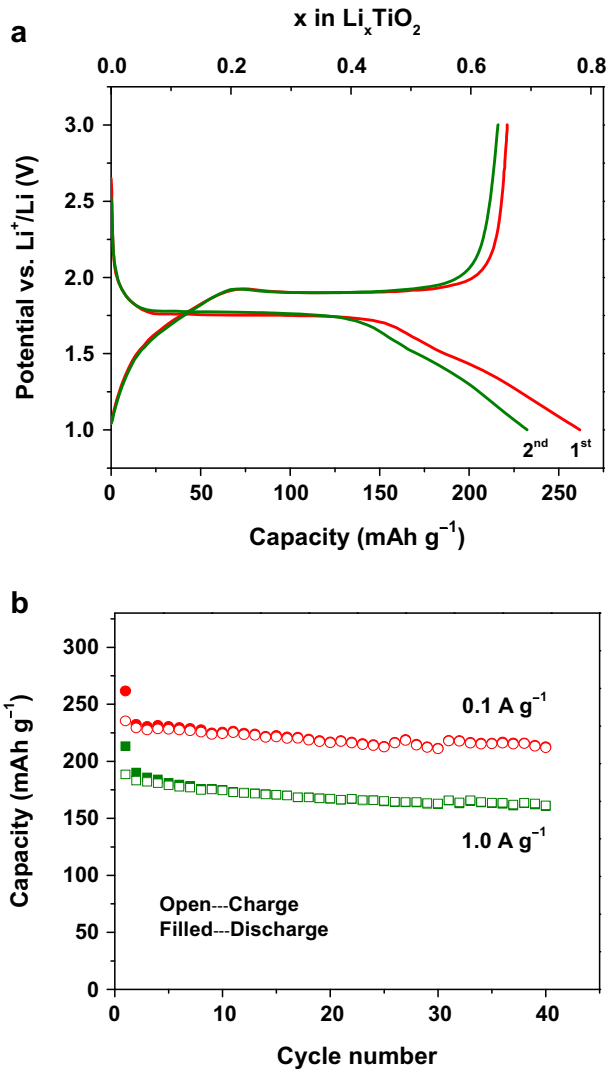

Fig. 5. (a) The initial two discharge/charge curves of mesoporous anatase TiO_2 rods at 0.1 A g^{-1}. (b) Cycling performance of mesoporous anatase TiO_2 rods at different current rates.

and 216 mAh g^{-1}, respectively, with the coulombic efficiency significantly improved. It is also noted that the distinct capacity decay between 1.78 and 1.0 V contributes to most of the irreversible capacities of the initial two cycles (Table 1). The strong Li–Li interaction in the lattice when x is over 0.5 in Li_xTiO_2 is the account for the capacity decay between 1.78 and 1.0 V with further lithium-ion insertion into $Li_{0.5}TiO_2$ [24]. In addition, it is noted that a small plateau around 1.4 V appears in the initial discharge curve. This plateau which might result from the insertion of very small amount of lithium-ions into irreversible sites in the anatase lattice and the side-reaction of lithium-ions with trace water absorbed [25], also contributes to the irreversible capacities.

Table 1

		Plateau voltage [V]	Capacity [mAh g^{-1}][a]			Capacity [mAh g^{-1}]	Coulombic efficiency
			I	II	III		
1st cycle	Discharge	1.75	24	129	109	262	85%
	Charge	1.90	27	126	68	221	
2nd cycle	Discharge	1.77	21	116	96	232	93%
	Charge	1.90	33	117	67	216	

[a] The capacities of the region above the plateau (I), of the plateau (II), and that below the plateau (III).

High rate capability and good cycleability are important properties of an electrode material for high power LIBs. Therefore, the cycling performance of the mesoporous TiO_2 rods is investigated at various current densities. Fig. 5b shows the variation of the specific discharge and charge capacities as a function of the cycling number at current densities of 0.1 and 1.0 A g^{-1}, respectively. Cycled at 0.1 A g^{-1}, the discharge and charge capacities of the mesoporous TiO_2 rods are quite high. After 40 cycles, a specific discharge capacity of 213 mAh g^{-1}, approximately 81% of the initial discharge capacity is retained. As expected, higher current densities result in relatively lower specific capacities. Cycled at a current density of 1.0 A g^{-1} (approximately 6C), the mesoporous TiO_2 rods show a discharge capacity of 213 mAh g^{-1} in the first cycle, corresponding to an insertion coefficient (x) of 0.64. The discharge capacity of mesoporous TiO_2 rods at a current density as high as approximately 6C is even superior over that of nanoporous anatase TiO_2 mesocrystals (approximately 205 mAh g^{-1} at 1C) [26], indicating the high rate capability of these rods. Good capacity retention is realized over extended cycling. A charge capacity of 161 mAh g^{-1}, approximately 85% of its initial charge capacity is retained after 40 cycles. The good capacity retention of mesoporous TiO_2 rods cycled at a current density of 1.0 A g^{-1} demonstrate the high rate capability and good cycleability of this material.

The high specific capacity, good rate capability and cycleability of the mesoporous TiO_2 rods constructed by anatase nanocrystals are attributed to the unique mesoporous structure and the crystalline nature of the rods. Tetragonal anatase TiO_2 provides fast lithium ion insertion/extraction pathways along the a and b axes, ensuring the high capacity and good reversibility. The mesoporous structure formed by the aggregation of anatase nanocrystals facilitates the transport of electrolyte within the electrode and shortens the diffusion distance for both electron and lithium-ions. The high specific surface area of the TiO_2 rods provides sufficient electrode-electrolyte contact interface. These structural features offer fast lithium insertion/extraction kinetics, leading to high rate capability. The high crystallinity of the anatase nanocrystals results in good cycling performance. In addition, during the calcination process, the amorphous walls of the mesoporous TiO_2 rods crystallize into well-connected anatase nanocrystals. The capacity decay caused by the dissociation of nanoparticles from the electrode surface during cycling may be avoided.

4. Conclusions

Mesoporous TiO_2 rods composed of highly crystalline anatase nanocrystals have been successfully fabricated via a template-free approach. The diameters of these rods range from 0.5 to 1.0 μm and the lengths from 5.0 to 10 μm, whereas the particle size of the TiO_2 nanocrystals in the rods is within 10–20 nm. The specific surface area and the pore size of the mesoporous rods are determined to be 53 m^2 g^{-1} and 9.0 nm, respectively. The obtained mesoporous TiO_2 rods exhibit a high initial discharge capacity of 262 mAh g^{-1} at 0.1 A g^{-1}. Cycling at 1.0 A g^{-1}, a capacity of 161 mAh g^{-1} is retained even after 40 cycles, indicating excellent cycling stability. The high electrochemical performance of the mesoporous TiO_2 rods is attributed to the unique mesoporous structure and the crystalline nature of the rods, which facilitate the transport of the electrolyte and improve the lithium-ion insertion/extraction kinetics. The mesoporous TiO_2 rods bear the potential to be used as a promising anode material for lithium-ion batteries with high energy and power densities.

Acknowledgments

This work was financially supported by the National Natural Science Foundation of China (91022019, 20901050, 21151002) and the National Basic Research Program (2011CB808703).

References

[1] M. Armand, J.M. Tarascon, Nature 451 (2008) 652–657.
[2] T. Ohzuku, Z. Takehara, S. Yoshizawa, Electrochim. Acta 24 (1979) 219–222.
[3] D.W. Murphy, R.J. Cava, S.M. Zahurak, A. Santoro, Solid State Ionics 9-10 (1983) 413–417.
[4] B. Zachau-Christiansen, K. West, T. Jacobsen, S. Atlung, Solid State Ionics 28-30 (1988) 1176–1182.
[5] D. Dambournet, I. Belharouak, K. Amine, Chem. Mater. 22 (2010) 1173–1179.
[6] Z. Yang, D. Choi, S. Kerisit, K.M. Rosso, D. Wang, J. Zhang, G. Graff, J. Liu, J. Power Sources 192 (2009) 588–598.
[7] Y. Wang, M. Wu, W. Zhang, Electrochim. Acta 53 (2008) 7863–7868.
[8] M.S. Wu, M.J. Wang, J.J. Jow, W.D. Yang, C.Y. Hsieh, H.M. Tsai, J. Power Sources 185 (2008) 1420–1424.
[9] Y. Zhang, H. Zheng, G. Liu, V. Battaglia, Electrochim. Acta 54 (2009) 4079–4083.
[10] M. Wagemaker, G.J. Kearley, A.A. van Well, H. Mutka, F.M. Mulder, J. Am. Chem. Soc. 125 (2003) 840–848.
[11] A. Fujishima, K. Honda, Nature 238 (1972) 37–38.
[12] B. O'Regan, M. Grätzel, Nature 353 (1991) 737–740.
[13] G.K. Boschloo, A. Goossens, J. Schoonman, J. Electrochem. Soc. 144 (1997) 1311–1317.
[14] K. Wang, M. Wei, M.A. Morris, H. Zhou, J.D. Holmes, Adv. Mater. 19 (2007) 3016–3020.
[15] D. Fattakhova-Rohlfing, M. Wark, T. Brezesinski, B.M. Smarsly, J. Rathouský, Adv. Funct. Mater. 17 (2007) 123–132.
[16] P. Kubiak, J. Geserick, N. Hüsing, M. Wohlfahrt-Mehrens, J. Power Sources 175 (2008) 510–516.
[17] K. Saravanan, K. Ananthanarayanan, P. Balaya, Energy Environ. Sci. 3 (2010) 939–948.
[18] X.F. Zhang, K.X. Wang, X. Wei, J.S. Chen, Chem. Mater. 23 (2011) 5290–5292.
[19] X.X. Zou, G.D. Li, K.X. Wang, L. Li, J. Su, J.S. Chen, Chem. Commun. 46 (2010) 2112–2114.
[20] X. Jiang, Y. Wang, T. Herricks, Y. Xia, J. Mater. Chem. 14 (2004) 695–703.
[21] S.J. Bao, Q.L. Bao, C.M. Li, D.Z. Li, Electrochem. Commun. 9 (2007) 1233–1238.
[22] Y. Xia, H. Takeshige, H. Noguchi, M. Yoshio, J. Power Sources 56 (1995) 61–67.
[23] G. Sudant, E. Baudrin, D. Larcher, J.-M. Tarascon, J. Mater. Chem. 15 (2005) 1263–1269.
[24] L. Kavan, J. Rathouský, M. Grätzel, V. Shklover, A. Zukal, J. Phys. Chem. B 104 (2000) 12012–12020.
[25] J. Xu, C. Jia, B. Cao, W. Zhang, Electrochim. Acta 52 (2007) 8044–8047.
[26] J. Ye, W. Liu, J. Cai, S. Chen, X. Zhao, H. Zhou, L. Qi, J. Am. Chem. Soc. 133 (2011) 933–940.